Construction and Building Materials 187 (2018) 519–530

Contents lists available at ScienceDirect

Construction and Building Materials

journal homepage: www.elsevier.com/locate/conbuildmat

Acoustic Emission behavior of thermally damaged Self-Compacting High Strength Fiber Reinforced Concrete

Hernán Xargay [a,b], Paula Folino [b], Nicolás Nuñez [a], Martín Gómez [a], Antonio Caggiano [b,c,*], Enzo Martinelli [d]

[a] Comisión Nacional de Energía Atómica (CNEA), Departamento ICES, Buenos Aires, Argentina
[b] Universidad de Buenos Aires, Facultad de Ingeniería, INTECIN (UBA-CONICET), Argentina
[c] Institut für Werkstoffe im Bauwesen, Technische Universität Darmstadt, Germany
[d] Università di Salerno, Dipartimento di Ingegneria Civile, Fisciano, SA, Italy

HIGHLIGHTS

- High temperature effects were investigated on SC-High Strength and Fiber-Reinforced Concrete.
- Steel fibers played a beneficial role in bridging the expansion of heat-induced cracks.
- Acoustic Emission (AE) measurements allow scrutinizing thermal damages in cementitious composites.
- AE activity was monitored for analyzing bridging fiber mechanisms in SCHSFRC.

ARTICLE INFO

Article history:
Received 24 April 2018
Received in revised form 4 July 2018
Accepted 21 July 2018

Keywords:
Acoustic Emission
Self-Compacting
High-Strength Concrete
Fiber-Reinforced Concrete
High temperature

ABSTRACT

This paper investigates the effect of high temperature on two different Self-Compacting (SC) cementitious composites. SC-High Strength (SCHSC) and Fiber-Reinforced Concrete (SCHSFRC) samples were tested in three-point bending after having been exposed to high temperature at 300 and 600 °C. Besides the conventional force-displacement response, Acoustic Emission (AE) activity was monitored during the bending tests with the aim to investigate the possible correlation between the fracture behavior, the rate of AEs and the influence of high temperature exposure. The tests clearly pointed out the effects of heat exposure. More specifically, SCHSC specimens showed a significant decay in mechanical properties as a result of thermal treatments. Then, a lower degradation was observed for the SCHSFRC after heat exposure at 300 °C, whereas the specimens exposed to 600 °C exhibited a tougher response than the corresponding SCHSC. The results showed that the effect of fibers played a beneficial role in bridging the expansion of heat-induced cracks developed in the concrete matrix during the exposure of specimens at high temperature. This bridging effect of fibers was observed also in terms of the AE activity: much less AE events were systematically registered for SCHSFRC specimens with respect to SCHSC ones, for a given value of the imposed Crack-Mouth-Opening-Displacement (CMOD). Therefore, AE measurements confirm their potential in scrutinizing the damage level in cementitious composites.

1. Introduction

Over the last decades, the use of Self-compacting High-Strength Concrete (SCHSC) in the construction industry has been expanding considerably. Significant advances in new materials, quality and mixture proportioning, e.g. chemical admixtures and mineral binders, have led to both obtaining outstanding flowability at the fresh state and increasing compressive strength at the hardened state. As a result of the lower water-cement ratio, the microstructure of SCHSCs has less permeability and porosity, with enhanced durability against harmful actions of the environment, hence, a longer service life. However, strength increase implies a less ductile mechanical behavior [1,2]. The addition of amounts between 30 and 80 kg/m^3 of steel fibers in concrete improves its energy absorption capacity and limits the propagation and width of cracks [3]. SCHSC is also characterized by a higher content of cement paste and a more compact microstructure than those of

* Corresponding author at: Institut für Werkstoffe im Bauwesen, Technische Universität Darmstadt, Germany.
E-mail addresses: hernanxargay@cnea.gov.ar (H. Xargay), pfolino@fi.uba.ar (P. Folino), nnunez@cnea.gov.ar (N. Nuñez), mpgomez@cnea.gov.ar (M. Gómez), acaggiano@fi.uba.ar (A. Caggiano), e.martinelli@unisa.it (E. Martinelli).

https://doi.org/10.1016/j.conbuildmat.2018.07.156
0950-0618/

Normal-Strength Concrete (NSC). Consequently, SCHSC could develop higher internal vapor pressure gradients under high-temperature exposure which allows to trigger microcracking and, sometimes, explosive detachment of parallel parts to the heated concrete surface. This phenomenon is called "spalling" and, although it can also occur in NSCs, it is more frequent and pronounced in High-Strength Concretes (HSCs) [4]. However, it was demonstrated that the incorporation of small amounts of polypropylene microfibers can partially mitigate this drawback [5–7].

The interest for investigating the behavior of concrete exposed to high temperatures has been motivated by two main reasons: fire resistance of tunnels and/or buildings and the nuclear facilities behavior. The design of new concrete demands to know their behavior under several environmental conditions, including for temperatures ranging between 20 °C and 800 °C [8,9]. Concrete exposed to high temperatures suffers chemical and physical changes, such as loss of moisture content, microstructure modification and aggregates decomposition which are mainly related to the reached maximum temperature of exposure [10]. Up to 200 °C no important changes take place in concrete mechanical properties due to the evaporation of the free and adsorbed water. Conversely, with increasing temperature (up to 500 °C), the average pore size grows up due to the loss of water and dehydration of hydrated calcium silicates (C-S-H). Specifically, reaching 450 °C, the calcium hydroxide ($Ca(OH)_2$) of the cement paste decomposes into calcium oxide (CaO_2) and water. Up to these temperatures, the aggregates are more or less stable, excepting the siliceous aggregates. Furthermore, over 500 °C, concrete chemical and physical changes become very important and irreversible: at 573 °C, the aggregates α-quartz crystalline phase transforms into β-quartz, resulting in deleterious expansions. A further increase in temperature up to 600 °C leads to the initiation of chemical decomposition in C-S-H, which is the main strengthening compound of cementitious matrix. Between 600 °C and 800 °C calcium carbonate ($CaCO_3$) dissociates. Moreover, after 800 °C all the hydration or chemically combined water has already been lost and the strength capacity becomes very low. Finally, at 1200 °C the solid compounds begin to melt [11]. However, concrete behavior subjected to high temperature does not only depend on the maximum temperature, but it is also affected by many environmental conditions, such as heating rate, temperature permanence time, cooling and humidity level, among others [9,10,12].

Several investigations have shown that thermal actions induce substantial modifications in cohesion and strength of concrete, which reduce both Young's modulus and Poisson's coefficient [13–17]. Concrete behaves in a more ductile manner increasing peak compressive strength deformation as temperature rises [18]. In addition, a slight increase in fracture energy released up to 400 °C has been observed, which decreases at higher temperature due to excessive thermal damage and the strong loss of tensile and compression strength [19,20]. Specifically, the experimental evidence for Self-Compacting Concrete (SCC) at high temperature shows that their mechanical properties are more seriously thermally degraded than traditionally-vibrated ones [17,21–24].

The actual state of damage of concrete can be scrutinized by means of non-destructive techniques, among which Acoustic Emission (AE) testing is gaining consensus within the scientific community [25]. In fact, AE is known as the spontaneous release of elastic energy in the form of transient elastic waves that occurs within the materials when stressed [26]. Hence, the waves contain information about internal behavior of the material [27]. Structural modifications such as cracks growth and friction are generated as the fracture process of concrete is progressing, which are associated with acoustic emissions. These elastic waves propagate from their sources to the surface where piezoelectric sensors convert them into electrical signals which can be subsequently processed by a specific electronic equipment. A set of relevant signal parameters can be calculated in order to characterize the digitalized AE waveforms. Therefore, AE technique has been used to monitor in real time laboratory mechanical tests of concrete specimens due to it great sensitivity to detect damage evolution from the very beginning [28–32]. Many investigations have been carried out in order to quantify the global damage level of reinforced concrete elements using AE-based parametric approaches. For this purpose, new indexes derived from conventional AE parameters have been defined: e.g., Calm ratio [33,34], Cumulative Signal Strength ratio [35,36], Relaxation ratio [37], b-value [38–40] and Improved b-value [41], among others. Moreover, AE can deliver useful information to detect, locate and infer the origin of the sources [30,42,43]. In this regard, several experimental results have been reported evidencing the close relationship between the AE features with the source cracking mode [44–47]. It has been pointed out that tensile fracture mode, characterized by opening mode I movements of the crack, results in AE signals with higher frequency and shorter rise time (defined as elapsed time from the first arrival to the peak amplitude). On the other hand, shear fracture mode waveforms, represented by a sliding mode II movement of the crack faces, show lower frequency and longer rise time and duration. Thus, AE events can be plotted in a bi-dimensional representation defined by the combined features of RA value (rise time over amplitude) and Average Frequency (AF) (counts over duration) to assess the cracking mode corresponding to the AE source.

This work reports the results obtained from three-point bending tests carried out on both SCHSC and SCHSFRC with the aim to investigate the influence of heat-induced damage on their cracking and post-cracking behavior. Both force-displacement relationship and AE activity were monitored during those tests. Thermal treatments were performed in an electric furnace at maximum temperatures of 300 and 600 °C. Steel macrofibers (0.76% in volume) and polypropylene microfibers (0.1%) were dispersed within the concrete matrix of the SCHSFRC mixture. It is important to remark that the adopted methods followed in this work mainly investigated the high temperature exposure at the material level and thus, the structural response at a fire scenario is out of the scope of this paper.

In the Authors' best knowledge, no experimental researches are available in the scientific literature reporting the fracture behavior of thermally damaged SCHSFRC specimens, tested in bending and related to AE activities. Indeed, the exiguous related results currently available refer to either Fiber Reinforced Concrete (FRC) [48–51] or thermally-treated concrete without steel fibers reinforcement [52–55]. Therefore, the results presented in this paper could be useful to researchers interested at studying the AE applicability limits as valuable tool in Structural Health Monitoring (SHM) for high responsibility structures, such as spent nuclear fuel storage facilities.

2. Materials and methods

This section summarizes the experimental activities related to the AE tests executed at the Laboratory of Materials and Structures of the University of Buenos Aires, Argentina. Further details on the extended experimental program and results of complementary mechanical tests can be found in [56]. The specimens for this experimental program were prepared adopting a unique dosage for the concrete matrix characterized by a water-to-binder ratio of 0.35. This mixture was designed to achieve an adequate flowability at the fresh state and, at the same time, a high-strength in hardened state.

2.1. Materials

The selected concrete constituents were early age high-strength Portland cement, finely Ground Granulated Blast Furnace Slag (GGBFS), three different fractions size of siliceous aggregates and a very high range polycarboxylate-based superplastizicer admixture. The mixture composition is detailed in Table 1. The

Table 1
Basic mixture composition per cubic meter.

Materials	Dosage [kg/m^3]
Cement	429.8
GGBFS	183.9
Water	214.6
Natural fine sand	281.1
Crushed sand	499.7
Crushed coarse aggregates	783.7
Superplasticizer	3.1

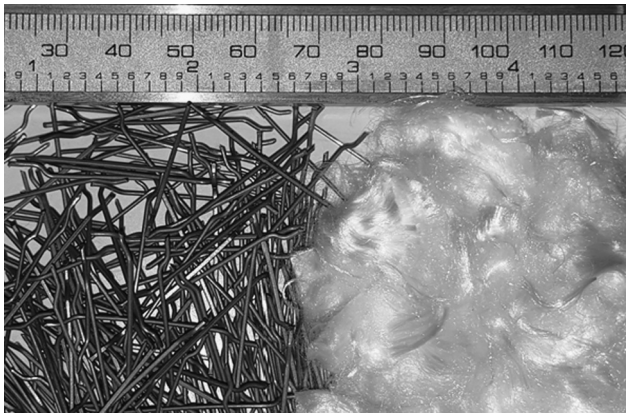

Fig. 1. Hooked-end steel macrofibers and polypropylene microfibers.

maximum nominal size of the coarse fraction was Φ_{max} = 9.50 mm and the overall Fineness Modulus (FM) resulting from the total aggregate mixture was FM = 4.29. The SCHSC mean uniaxial compressive strength was 97.9 MPa, obtained from three cylinders of 100 mm diameter and 200 mm height.

According to their length, fibers for concrete are usually classified in micro- and macrofibers. The former are used to reduce drying shrinkage and to prevent the spalling effect, while macrofibers increase the ductility and restrict the growth of macrocracks [57]. In this research, FibroMac 12 monofilament polypropylene microfibers (0.1% in volume) and Wirand FS3N steel macrofibers (0.76% in volume) were used (Fig. 1). Main technical data for both fibers are shown in Table 2.

The following mixture labels were adopted based on the SCHS concrete composition and maximum temperature exposure:

- SCHSC20: plain concrete without exposure to high temperature;
- SCHSC300: plain concrete exposed to 300 °C;
- SCHSC600: plain concrete exposed to 600 °C;
- SCHSFRC20: fiber-reinforced concrete, without exposure to high temperature;
- SCHSFRC300: fiber-reinforced concrete exposed to 300 °C;
- SCHSFRC600: fiber-reinforced concrete exposed to 600 °C.

2.2. Methods

Concrete batches were realized in a laboratory pan type concrete mixer with vertical axis. Three beams (150 × 150 × 600 mm^3) were molded for each concrete batch. Due to self-compacting characteristics, molds were filled in a single pour and no further compaction was carried out. The specimens were thus demolded after 24 h and cured until 28 days-age immersed in water at 20 °C temperature. Subsequently, they were stored in laboratory conditions for moisture stabilization up to heat treatment.

Concrete specimens labeled as SCHSC300, SCHSC600, SCHSFRC300 and SCHSFRC600 were individually subjected to 300 and 600 °C maximum temperature in a vertical electric oven for 3 h (Fig. 2a). The adopted heating rate (Fig. 2b) was

(a)

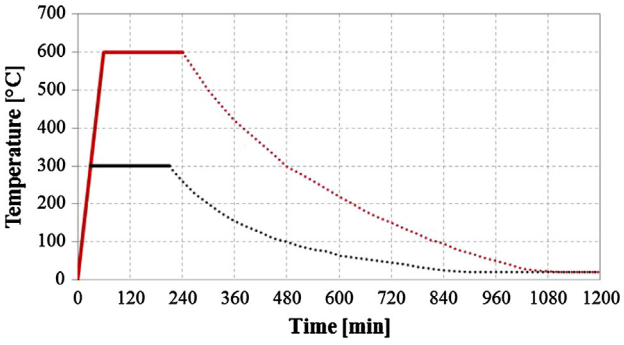

(b)

Fig. 2. (a) Electric furnace and (b) heating curve.

10 °C/min. Then, cooling was done slowly into the furnace and the specimens were removed 24 h later. Spalling phenomena never occurred, however, numerous cracks were observed on the surface of the treated samples, especially for those heated at 600 °C. Nevertheless, fiber-reinforced concrete specimens showed better surface integrity. All the specimens were weighted immediately before and after the heat treatments. The mean relative weight loss was 6.8% for SCHSC300, 6.7% for SCHSFRC300, 8.0% for SCHSC600 and 8.2% for SCHSFRC600. It is concluded that the effect of the addition of fibers in weight loss was totally negligible. These results are also in agreement with those reported by [21], where two different mixtures of SCC were treated at a heating rate of 1 °C/min.

After the aforementioned operation a notch of 25 mm deep were cut at mid-span of the beams with a diamond-edged saw. Then, the flexural behavior was evaluated in three-point bending test (TPB) 30 days after heat treatments by means of a 2000 kN maximum capacity testing machine with closed-loop control according to RILEM TC 162-TDF recommendations [58]. The beam span was 500 mm and load was applied in the central notched section. Test control was performed by means of a Crack Mouth Opening Displacement (CMOD) feedback-control. CMODs were measured through a clip gauge sensor with the aim of characterizing the post-peak tensile behavior. The CMOD rate was 0.05 mm/min until 0.25 mm reading was reached and then 0.20 mm/min up to the test end. Load measurement was performed through a 300 kN capacity load cell.

Table 2
Fibers main technical data [65,66].

Fibers	Diameter [mm]	Length [mm]	Tensile Strength [MPa]	Elastic Modulus [GPa]	Specific weight [kN/m^3]	Content [kg/m^3]
Steel	0.750	33	1100	200.0	78.5	60.0
Polypropylene	0.032	12	400–500	3.5–3.9	9.1	0.9

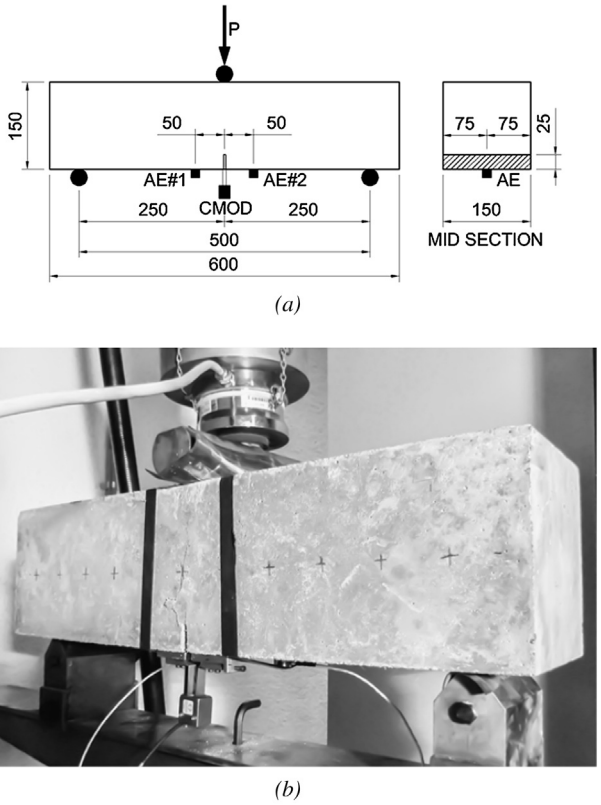

Fig. 3. Three-point bending test setup: (a) beam geometry (distances in mm) and (b) sensors arrangement.

The tests were continuously monitored by AE testing system. For this purpose, a PAC AE system PCI-2 board with two R15D 150 kHz resonant sensors and 2/4/6 preamplifiers with 40 dB gain were used. Although for field inspections in real structures, and with large separation/distance between the sensors, it is widely recommended to use low frequency resonant sensors, 150 kHz sensors were used in this experimental campaign for two main reasons: (a) the specimens and distances between the sensors were small, thus, the crack tip were in the range of 6–17 cm, and (b) sensors with 150 kHz resonant frequency are more adequate to supply good sensitivity and to reduce background noise. Moreover, the used sensors with external preamplifier are more sensitive than low frequency resonant sensors with included preamplifier. Thus, the choice of using 150 kHz sensors was the result of a balance between sensitivity and attenuation for this particular experimental setup.

The sensors were symmetrically located at 5 cm of each side from the notch axis, on the bottom surface of the beam, as shown in Fig. 3. Rubber acoustic insulations were placed at the support in order to reduce friction noise. Vaseline as coupling media at sensors-concrete interface was used. Before performing each flexural test, preliminary measurements of the background noise and signal attenuation trials were carried out by generating Hsu-Nielsen artificial sources at different points on the beam front surface. A measurement threshold of 45 dB and a frequencies filter of 20–400 kHz were preset in the equipment. The AE adopted sampling frequency was 2 MHz. In order to extract spurious hits without physical sense, AE raw data were firstly pre-filtered by magnitude of AE features. Then, to corroborate that emission sources were generated at the central volume of the beams, data were filtered by a zone location criterion based on time of arrival. For the specimens treated at 600 °C, it was found that the isotropic medium hypothesis (apparent wave velocity) did not provide accurate results due to high amounts of inhomogeneous thermal damages. Hence, in those cases, only the magnitude of AE features was used for data filtering.

3. Results and discussion

3.1. Mechanical performance

Figs. 4–6 show the Load-CMOD behavior for the reference temperature and thermal treatments at 300 °C and 600 °C, respectively. In each graph, the black line represents the average response of the three tests, while the gray envelope area indicates

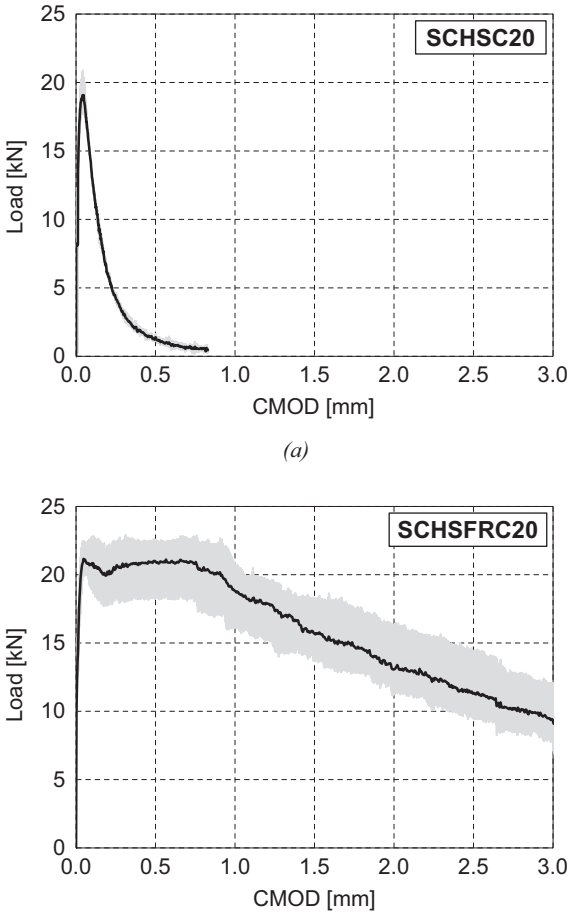

Fig. 4. Load vs CMOD at reference temperature (20 °C): (a) SCHSC and (b) SCHSFRC.

the experimental scatter. The fibers random distribution and cracks induced by thermal conditioning are some of several factors, besides the natural heterogeneity of concrete behavior, which contributes with the dispersion of results.

As expected, the presence of fibers results in a much higher toughness of the SCHSFRC with respect to SCHSC (Fig. 4). Conversely, the pre-peak branch and the cracking strength, which are mainly related to the matrix properties, were almost unaffected by the presence of fibers, as they mainly start working after the matrix cracking [59]. It is also observed that the maximum CMOD achieved was less than 1.5 mm for SCHSC20, contrarily in the case with fibers, the beams still had load bearing capacity even for 3.0 mm at the end of the test.

Peak load reduces for 300 °C maximum temperature treatment especially when plain concrete specimens (SCHSC300) were analyzed. Conversely, the bridging action of fibers is still effective, as specimens SCHSFRC300 exhibited a barely plastic response, though with a lower cracking strength due to the heat-induced degradation in the concrete matrix (Fig. 5).

Finally, a strong degradation of the mechanical behavior can be observed in the case of specimens pre-exposed to 600 °C (Fig. 6). On the one hand, two of three SCHSC specimens failed abruptly at peak load for plain concrete and, therefore, it can be said that 600 °C is an extreme temperature for plain SCHSC. Fracture occurred near the notches through preexisting thermal cracks, in both cases for CMOD less than 0.25 mm, resulting in a very low energy absorption capacity. Hence, only one complete result on SCHSC600 including post peak is reported in Fig. 6a: its flexural

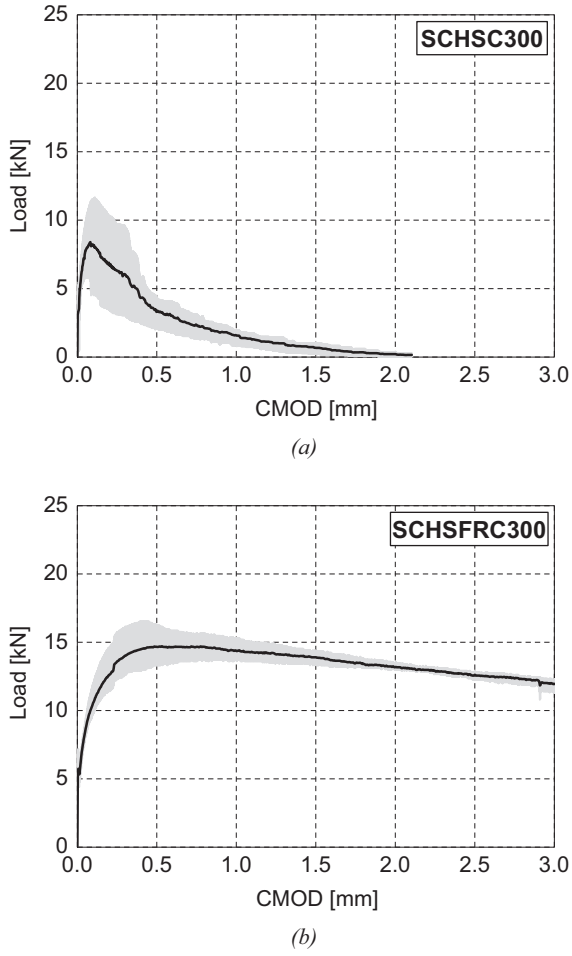

Fig. 5. Residual Load vs CMOD curve after 300 °C: (a) SCHSC and (b) SCHSFRC.

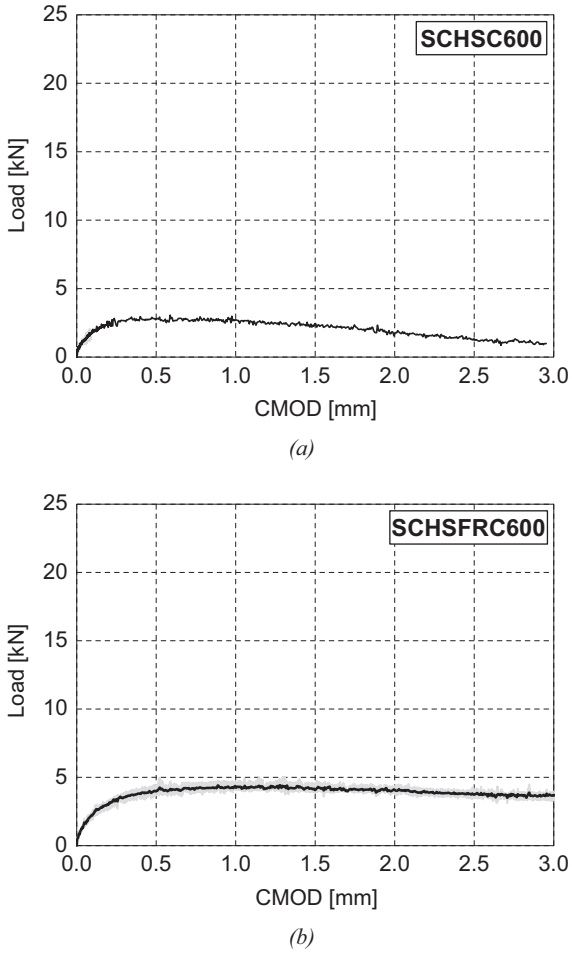

Fig. 6. Residual Load vs CMOD curve after 600 °C: (a) SCHSC and (b) SCHSFRC. Only one test for SCHSC600 was stably completed.

strength is about 15% of the one average determined for SCHSC20. On the other hand, all SCHSFRC600 specimens behaved in a similar manner, though their cracking strength was about 20% of SCHSFRC20 while the bridging effect of fibers was much weaker than the other analyzed cases (20 and 300 °C).

In order to characterize and compare the tensile behavior of fiber-reinforced concretes, the RILEM recommendation TC 162-TDF defines representative flexural parameters that can be obtained from the Load-CMOD curve. Particularly, these parameters are: the flexural strength $f_{fct,L}$ (corresponding to the highest value of the load (F_L) in the range of CMOD 0.05 mm), the energy absorption capacity due to the plain concrete D^b_{BZ}, the energy absorption capacity due to the influence of fibers $D^f_{BZ,2}$ and $D^f_{BZ,3}$, the equivalent flexural tensile strength ($f_{eq,2}$ and $f_{eq,3}$) and the residual flexural tensile strength $f_{R,1}$ (CMOD = 0.5), $f_{R,2}$ (CMOD = 1.5) and $f_{R,3}$ (CMOD = 2.5). In structural engineering applications, $f_{R,1}$ is accepted to be relevant for the serviceability limit state while $f_{R,3}$ is related for ultimate limit state. Table 3 summarizes the flexural parameters aforementioned. For the case of plain concrete, the fracture energy G_f was calculated following RILEM recommendation TC 50-FCM [60] and D^b_{BZ} was evaluated as the total area under the Load-CMOD curve.

Fig. 7 shows two X-ray images corresponding to the same sample and rotated 90 degrees. The specimen used for this descriptive purpose ($75 \times 75 \times 250$ mm^3) was sawn from one beam after been tested to make it compatible with the portable X-ray equipment. The images revealed that the fibers are uniformly distributed in the concrete matrix despite being a self-compacting concrete. Preferential orientations are only observed in the vicinity of the specimen faces that were in contact with the steel mold.

Fig. 8 shows photographs of the resulting failure faces and paths of three-point bending tests for SCHSC and SCFRHSC. Visual inspection of fracture surfaces of SCHSC specimens (Fig. 8a) allowed distinguishing color changes related with maximum temperature of exposure. Granitic coarse aggregate shifted from dark bluish-grey

Table 3
Flexural parameters of the different mixtures after exposed to temperature according to RILEM TC 162-TDF and 50-FMC.

Concrete Mixture	F_L [kN]	$f_{fCt,L}$ [MPa]	f_{max} [MPa]	G_f [N/m]	D^b_{BZ} [Nmm]	$D^f_{BZ,2}$ [Nmm]	$D^f_{BZ,3}$ [Nmm]	$f_{eq,2}$ [MPa]	$f_{eq,3}$ [MPa]	$f_{R,1}$ [MPa]	$f_{R,2}$ [MPa]	$f_{R,3}$ [MPa]
SCHSC20	19.1	6.1	6.1	202	3672	–	–	–	–	–	–	–
SCHSFRC20	21.1	6.7	6.7	–	3834	12004	45091	7.7	5.8	6.7	5.0	3.6
SCHSC300	8.2	2.6	2.6	290	4931	–	–	–	–	–	–	–
SCHSFRC300	8.5	2.7	4.7	–	2285	8009	39285	5.1	5.0	4.7	4.4	4.0
SCHSC600	1.3	0.4	0.8	133	2206	–	–	–	–	–	–	–
SCHSFRC600	1.7	0.5	1.4	–	511	2129	11567	1.4	1.5	1.3	1.3	1.2

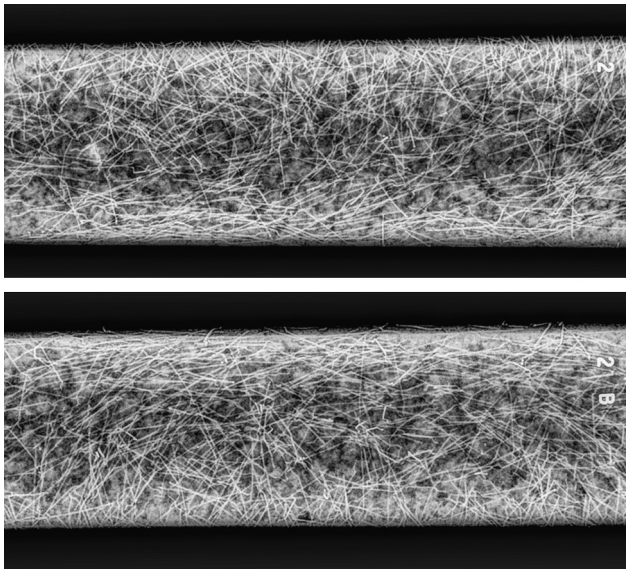

Fig. 7. X-ray images showing distribution of steel fibers in the same concrete sample and rotated 90 degrees.

at 20 °C and 300 °C to a lighter shade of grey, pink and white at 600 °C. Meanwhile, mortar phase color varied from normal grey to yellowish-grey at 300 °C and to darker grey at 600 °C with a remarkable increasing of porosity and friability. Another temperature effects can also been detected on the fracture surfaces: at 20 °C and 300 °C the crack paths fractured the aggregates while at 600 °C cracks go mainly through the interface between cement paste and aggregates, as it is usually occurring in non-thermally damaged NSC. From Fig. 8b and c, it can be highlighted that the tortuosity of crack paths was increased with temperature for both SCHSC and SCHSFRC. Moreover, for SCHSFRC600 the matrix stiffness weakening and the fibers bridging action generated several path direction changes, ensuring structural integrity of the specimens.

3.2. AE energy behavior

In the following "AE energy" refers to the Measured Area under the Rectified Signal Envelope (MARSE). The AE energy evolutions for the three thermal scenarios are shown in Figs. 9–11. Again, the average response of three tests repetitions with their dispersion is presented, with the exception of SCHSC600 as was explained before. Similar tendencies were observed in the cumulative curves corresponding to different AE parameters such as Counts, Duration, Amplitude and Signal Strength when expressed in their relative values. The AE energy is often selected to represent the magnitude of source event rather than other AE parameters (e.g. hits) because it is a function of both duration and amplitude of the signal. Furthermore, it is also less sensitive on threshold setting and operating frequency [61]. For the sake of brevity, only the cumulative AE energy as representative parameter of one channel is presented in this subsection. It can be noticed that AE results dispersion was increased with temperature. Thermal cracks were randomly distributed along the specimens and it greatly affected the fracture path development.

Fig. 12 shows the average Load-CMOD curve with the average cumulative AE energy response for the SCHSC20 and SCHSFRC20 specimens. Similarly, Figs. 13 and 14 reproduce the concretes performance after the heat treatments. Very few AE energy was recorded during the pre-peak branch in comparison to the post-peak (softening) branch for the cases of reference temperature, i.e. 20 °C (Fig. 12). This behavior can be explained due to microcracks growth in the intact cement matrix which are very low in comparison with the macrocracks localization development. Nevertheless, for SCHSFRC300 this behavior is quite different. Fig. 13 highlights that already a 30% of the AE energy recorded during the tests were released before reaching the maximum load. It

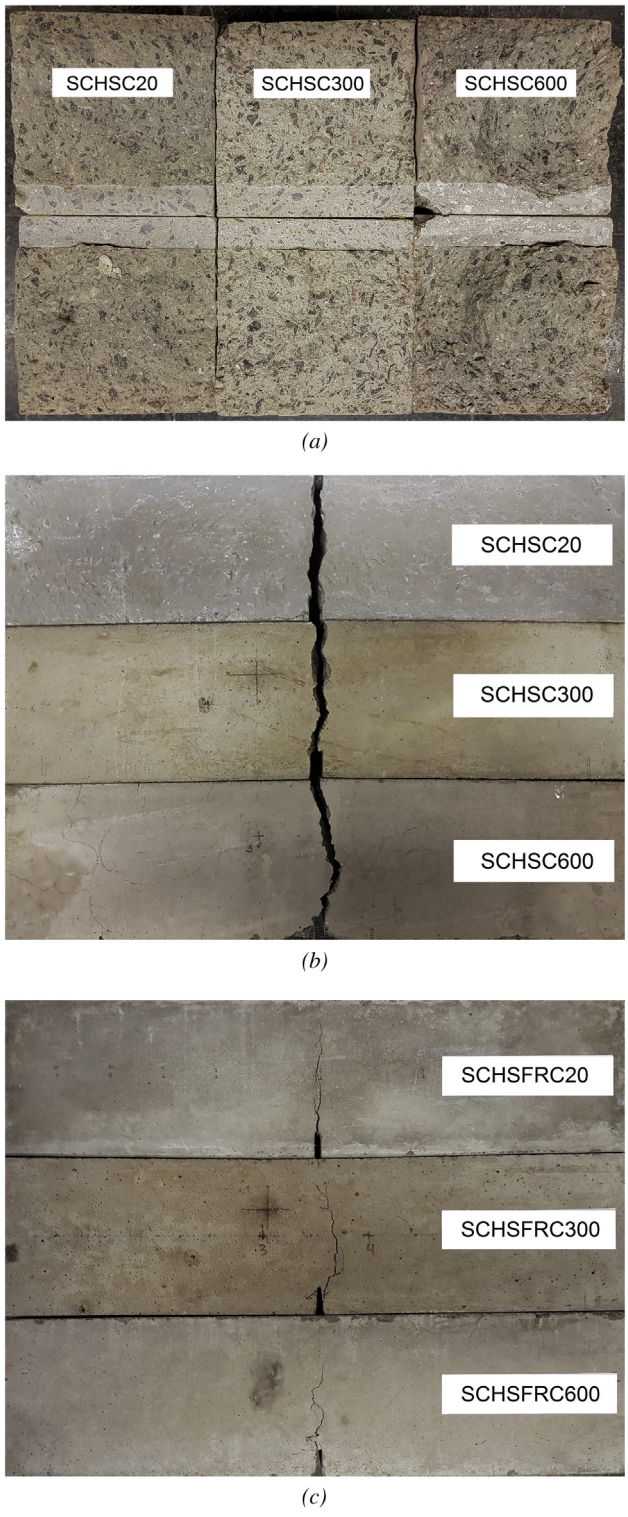

Fig. 8. (a) Fracture surface aspect of SCHSC, crack patterns of (b) SCHSC and (c) SCHSFRC.

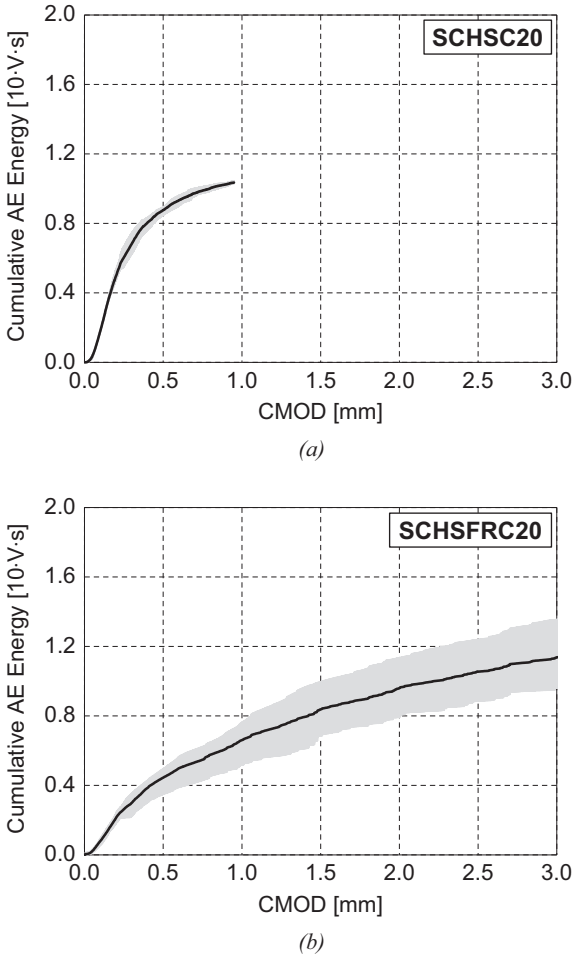

Fig. 9. Cumulative AE Energy parameter vs CMOD at reference temperature (20 °C): (a) SCHSC and (b) SCHSFRC.

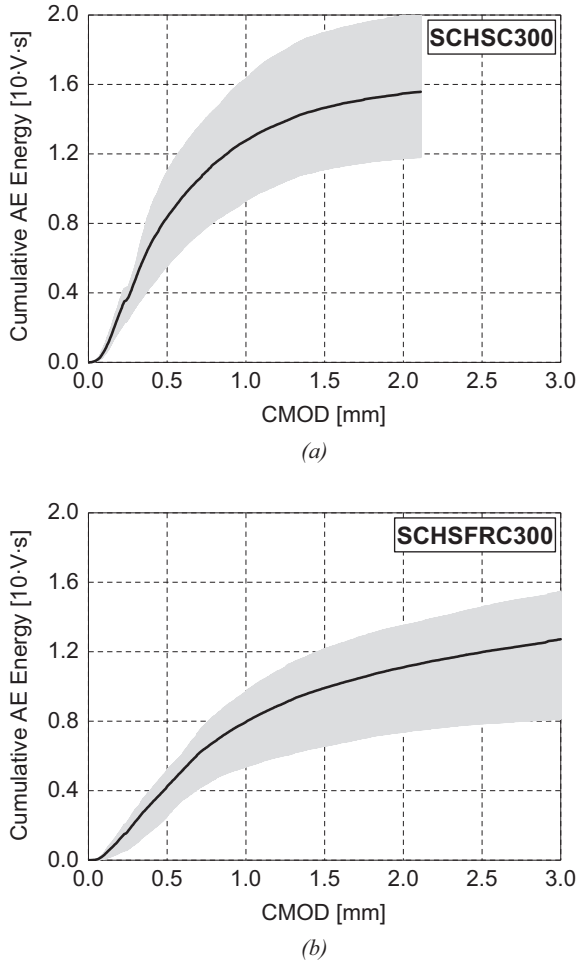

Fig. 10. Cumulative AE Energy parameter vs CMOD after 300 °C: (a) SCHSC and (b) SCHSFRC.

seems that the fibers action greatly contributes to withstand the loss of cohesion of the matrix due to the thermal degradation and increase the bearing capacity of the beam.

In all temperature scenarios, the AE rate is higher in plain concrete, reaching towards the test end with similar cumulative amounts. Therefore, for different CMOD values less than 2.0 mm, the cumulative AE is higher in SCHSC than in SCHSFRC. In the Authors understanding, this phenomenon was due to the fact that when applying a given CMOD, the fibers oppose to growing and coalescence of microcracks and, hence, less AE is released in SCHSFRC than in plain concrete. This is in good agreement with the conclusion by Rossi et al. [62], since they evidenced that the localized forces due to steel fibers mainly helps to delay the formation of microcracks, but they cannot prevent it. Cumulative AE curve slope flattens as the cracking develops in concrete matrix. However, AE continued to be recorded due to the friction caused by the interworking of the aggregates, the interaction between the new surfaces of the matrix and the fibers pullout mechanisms. AE behavior during CMOD controlled tests is significantly different from that typically observed in plain concrete where test control is performed through stroke displacement [49,50,55]. In such tests, plain specimens abruptly fail when the maximum load is reached, generating an instantaneous large amount of AE activity.

Taking into account that concrete serviceability limit states design rules restrict crack openings up to a maximum of 0.40 mm for environmental normal exposure [63], the amount of cumulative AE that can be related to concrete damage level, was significantly lower for SCHSFRC than for SCHSC. This means that, after crack opening, fibers are capable to "delay" the cracking process development throughout the concrete matrix. This concept can be thus identified with the AE technique.

Concrete samples after 600 °C showed comparatively lower AE amount and amplitude especially at the beginning stage of the tests. In those specimens, the inner structure of the specimens was degraded and had multiple cracks as result of the thermal treatment and, therefore, an important irreversible release of internal energy manifested as AE [52]. Then, when testing the beams, such energy is no longer available. Moreover, preexisting thermal cracks dampen the propagation of AE waves through the material and, hence, attenuate AE signals.

Finally, Figs. 15 and 16 aim at further highlighting the effect of temperature on the bending response of the two series of specimens of SCHSC and SCHSFRC. Specifically, Fig. 15 shows that the elastic response of SCHSC300 is almost overlapped to that one of the reference material. AE keeps producing in the post elastic range for SCHSC300, as a more gradual cracking process develops in these specimens due to the preexistence of heat-induced micro-cracks that progressive coalesce during the loading process. Conversely, the extremely weak response observed for SCHSC600 leads to few AE events, as the heat-induced micro-cracks have already severely weakened the concrete matrix continuity.

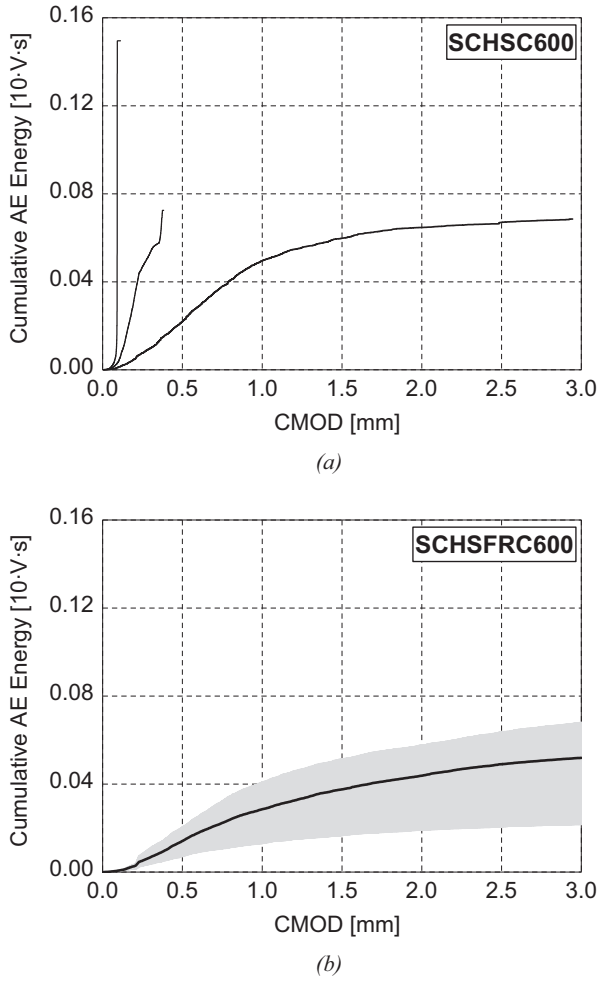

Fig. 11. Cumulative AE Energy parameter vs CMOD after 600 °C: (a) SCHSC and (b) SCHSFRC.

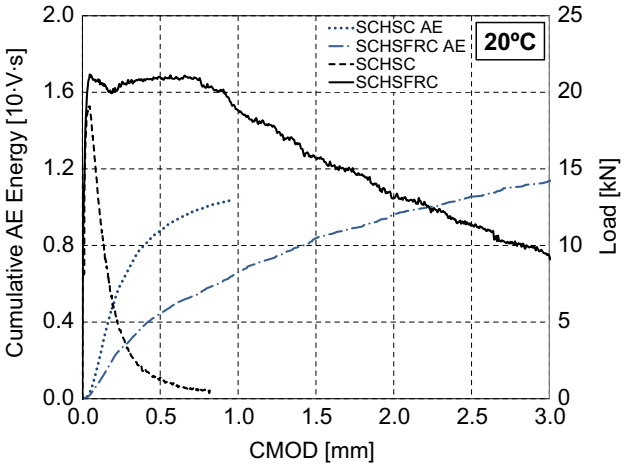

Fig. 12. Load and cumulative AE Energy vs CMOD behavior at reference temperature.

The obtained results of cumulative total amount of AE energy seem to show~~ed~~ a direct correlation with the fracture energy in plain concrete. Related to the reference case (20 °C), the fracture energy increased 44% at 300 °C due to greater tortuosity of the

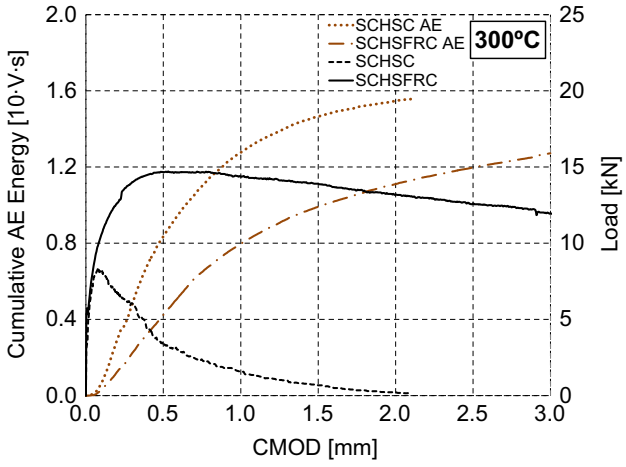

Fig. 13. Load and cumulative AE Energy vs CMOD residual behavior after 300 °C.

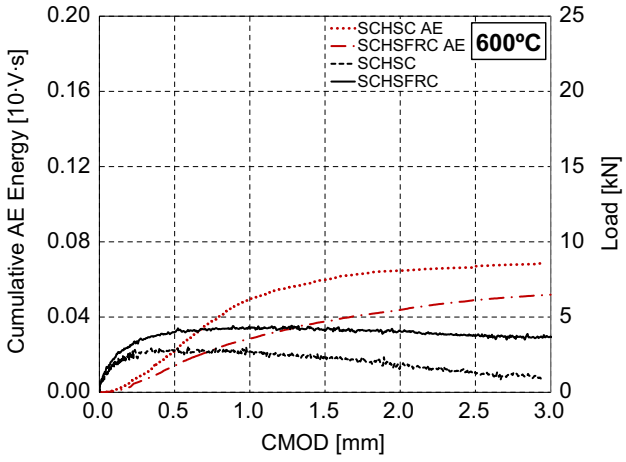

Fig. 14. Load and cumulative AE Energy vs CMOD residual behavior after 600 °C. AE data was intentionally rescaled.

fracture and decreased 34% at 600 °C due to the severe thermal damages (Table 3). This behavior is in agreement with the conclusions reported by some authors in literature [19,20]. On the other hand, the total AE energy grew 50% at 300 °C and reduced 93% at 600 °C.

Fig. 16 illustrates that fibers are capable to make cracking process almost overlapped for SCHSFRC20 and SCHCFRC300; however, the response of SCHSFRC600 is significantly affected by heat-induced damage, as already observed for SCHSC600 specimens. In opposition with plain concrete, SCHCFRC does not presented a clear relationship between AE energy and energy absorption capacity.

Finally, it is remarked that no comparisons can be proposed with other results available in the literature. To the Authors' best knowledge, other available data are obtained from tests carried out by different experimental procedures. Specifically, some results correspond to different mechanical tests, others to non-thermally treated specimens and, in most of the cases, to different AE equipment layouts and/or experimental setups.

3.3. AE frequency and RA value evolutions

Fig. 17 shows the histograms of RA value vs. average frequency of AE hits for all the analyzed concrete mix composition and

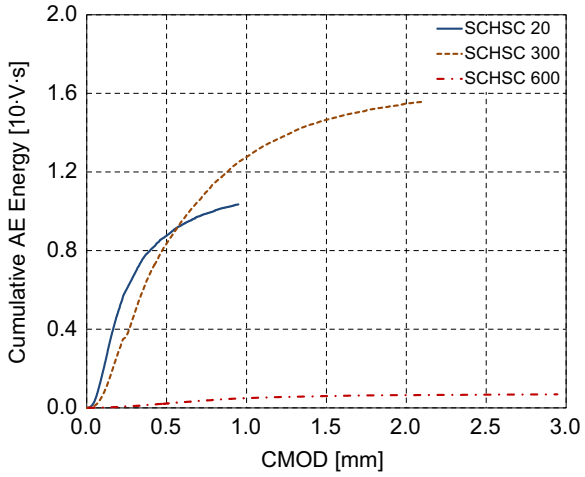

Fig. 15. Cumulative AE energy vs CMOD: SCHSC specimens.

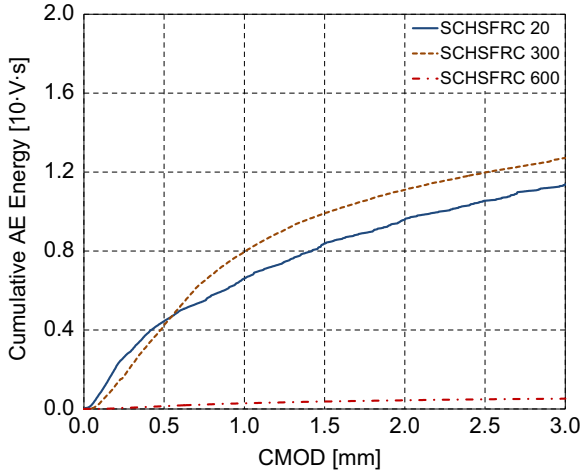

Fig. 16. Cumulative AE energy vs CMOD: SCHSFRC specimens.

temperature scenarios. The moving average of the RA value and the average frequency of 100 hits have been represented in order to smooth out scattering. The adopted criterion for a moving average of 100 hits was chosen as result of a previous sensitive study on AE data analysis. Trial examples performed with 25, 50, 75, 100, 150 and 200 hits were done. It was found that the plotted data become smooth and stable from 100 hits. This is also in accordance with RILEM TC 212-ACD [64] that recommends the adoption of more than 50 hits.

The plots distribution indicates that as the temperature grows up, the AE events decrease in frequency and increase in RA. This can be visualized by the progressive displacement of the AE cluster to the right and down corner in the figures. The tendency is evidenced both in SCHSC and SCHSFRC, and clearly points out that as concrete thermal degradation is more severe, the cracking behavior shifts to more mixed fracture modes. This is consistent with the observed increasingly tortuous fracture morphology.

Moreover, if the effect of the incorporation of fibers is analyzed, an increase of the RA value and the AF (although slightly in this case) is observed. This indicates that the fibers tend to modify the cracking modes activating the mixed modes as well. This was also supported by the fracture pattern aforementioned. Finally, Fig. 18 illustrates this behavior representing the peak frequency distribution of AF and RA value.

4. Conclusions

Self-compacting high strength concrete samples with and without hybrid steel/polypropylene fibers have been investigated in this work. Specifically, test specimens were exposed to maximum temperatures of 300 and 600 °C and, then, tested in bending. Both load-displacement response and AE activity were monitored during those tests.

On the one hand, the mechanical behavior allows to establish the following concluding remarks:

- peak flexural strength is significantly affected by temperature, though the fiber reinforcement shifts the residual flexural behavior;
- a remarkable nonlinearity can be observed in the bending response, as a consequence of matrix stiffness degradation due to high temperatures exposures;
- the fracture energy of SCHSC slightly increased for 300 °C and strongly decreased for 600 °C samples;
- fiber-reinforced concrete specimens continued to have considerable residual energy absorption capacity after the heat treatment, even at 600 °C.

On the other hand, AE measurements highlighted the following remarks:

- the bridging action of fibers restrain cracks propagation, which results in cumulative AE energy being released in SCHSFRC also during advanced stages of the post-cracking response and CMOD values;
- load-induced macro-cracks that are generated from pre-existing heat-induced micro-cracks, produce in SCHSFRC a smaller amount of AE hits with smaller amplitude than in plain specimens;
- in SCHSC, the recorded cumulative AE energy relatively grew up from 20 °C to 300 °C and declined for 600 °C as a result in the change of fracture energy due to heat-exposure;
- although the incorporation of fibers increased considerably the energy absorption capacity, the AE energy did not grow within the analyzed CMOD ranges, these latter chosen as representative for the useful life of a concrete structure;
- increasing thermal damages shifted the cracking modes to shear and mixed modes, characterized by a progressive decrease in average frequency and increase in RA value;
- incorporation of fibers in concrete slightly affects the AE features, changing to mixed modes, mainly increasing the RA values;
- advanced stages of cracking, produced by both thermal and mechanical process, constitute a limitation to the application of AE, as cracks dampen the AE signals.

Finally, the experimental results obtained from this study confirm the promising non-destructive AE technique for scrutinizing the actual level of damage. Analysis of different concrete composites, possible subjected to high temperature exposures and with fiber reinforcements were deeply investigated. Future research steps will aim at extending this procedure to other stress state conditions (i.e., uniaxial compression, triaxial compression and mixed modes of fracture) and to calibrate/connect the AE measurements together with the fracture mechanics parameters employed in a

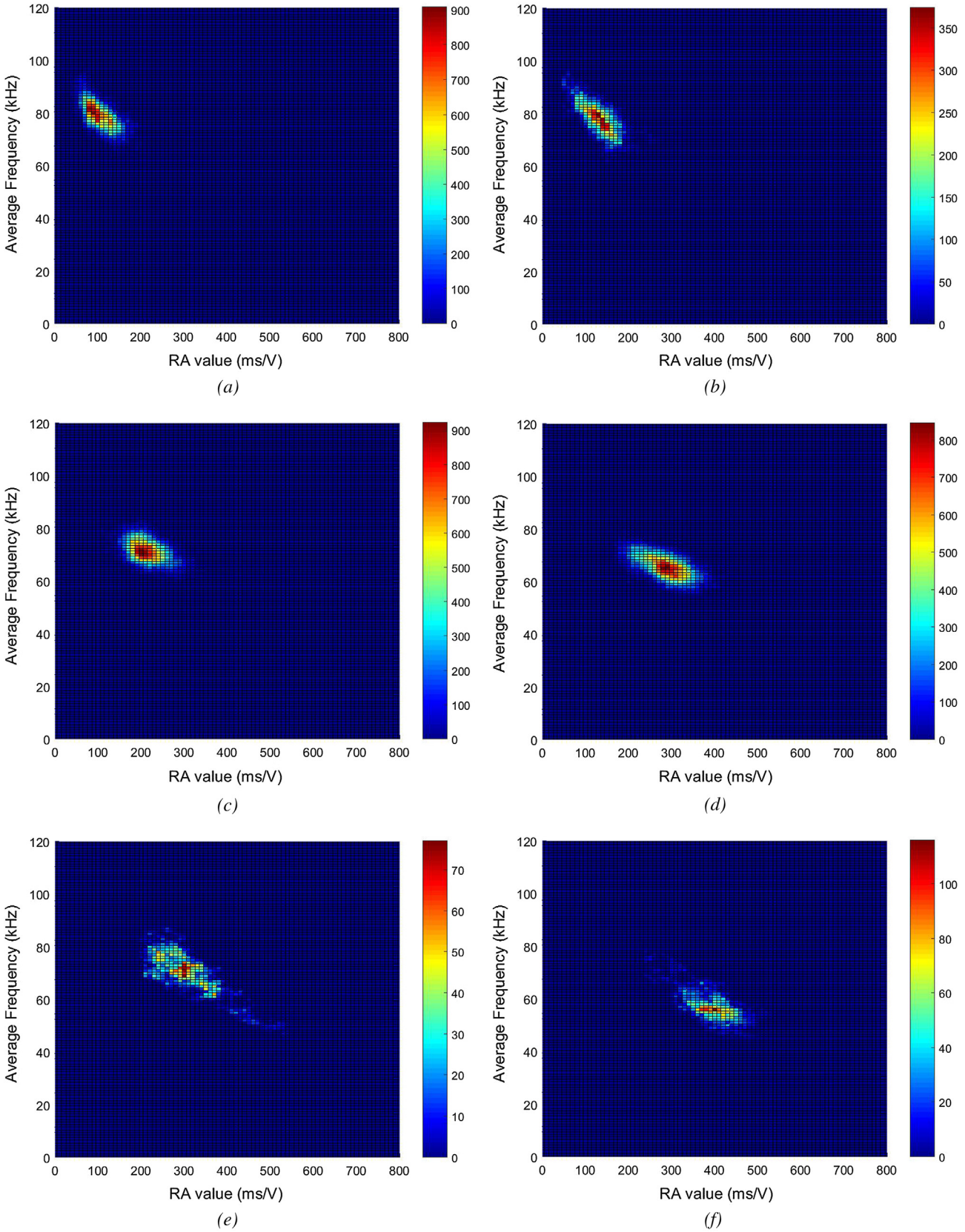

Fig. 17. 2D histograms of RA value – Average frequency for specimens corresponding to (a) SCHSC20, (b) SCHSFRC20, (c) SCHSC300, (d) SCHSFRC300, (e) SCHSC600, and (f) SCHSFRC600.

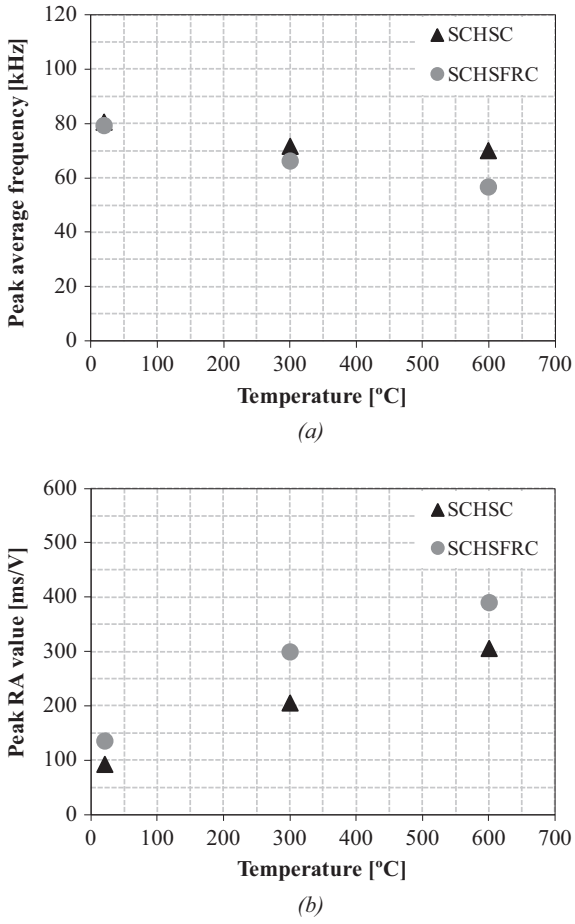

Fig. 18. Temperature evolutions of (a) Peak frequency distribution of AF and (b) Peak RA value.

constitutive model capable to predict the stress-crack opening displacements of FRC beams exposed to high temperatures.

Conflicts of interest

There are no potential conflicts of interest, including specific financial interests, relationships and affiliations relevant to the subject matter of the manuscript.

Acknowledgements

Contribution from the staff of the Laboratory of Materials and Structures of the University of Buenos Aires (UBA) is gratefully acknowledged, particularly Dr. L. Fernandez Luco for his valuable advices. Also, the authors are grateful to Eng. G. Fornasier (Lomax-InterCement) for providing raw materials, Eng. L. Sambataro for his collaboration with the experimental program and Eng. J. Scopelliti and E. Olivar Godaz (CNEA-ENDE) for the X-ray images.

The financial support of the "National Atomic Energy Commission of Argentina" (CNEA) and the SUPERCONCRETE Project (www.superconcrete-h2020.unisa.it), funded by the European Union (H2020-MSCA-RISE-2014, No. 645704) are also acknowledge. The Alexander von Humboldt-Foundation is also acknowledged for funding the temporary research position of Dr. A. Caggiano at the Institute of Construction and Building Materials - TU-Darmstadt under the research grant ITA-1185040-HFST-(2CENENRGY project).

References

[1] ACI Committee 363 – ACI 363R-10. (2010). Report on High-Strength Concrete. Reported by ACI Committee 363.
[2] E. Martinelli, A. Caggiano, H. Xargay, An experimental study on the post-cracking behaviour of Hybrid Industrial/Recycled Steel Fibre-Reinforced Concrete, Constr. Build. Mater. 94 (2015) 290–298.
[3] ACI Committee 544 – ACI 544.1R-96. (Reapproved 2009). State-of-the-Art Report on Fiber Reinforced Concrete. Reported by ACI Committee 544.
[4] C. Castillo, A.J. Durrani, Effect of transient high temperature on high-strength concrete, ACI Mater. J. 87 (1990) 47–53.
[5] C.-G. Han, Y.-S. Hwang, S.-H. Yang, N. Gowripalan, Performance of spalling resistance of high performance concrete with polypropylene fibers contents and lateral confinement, Cem. Concr. Res. 35 (9) (2005) 1747–1753.
[6] A. Noumowe, Mechanical properties and microstructure of high strength concrete containing polypropylene fibres exposed to temperatures up to 200 °C, Cem. Concr. Res. 35 (11) (2005) 2192–2198.
[7] A. Behnood, M. Ghandehari, Comparison of compressive and splitting tensile strength of high-strength concrete with and without polypropylene fibers heated to high temperatures, Fire Saf. J. 44 (8) (2009) 1015–1022.
[8] RILEM Technical Committee 200-HTC: Mechanical concrete properties at high temperatures – modelling and applications. Part 1: Introduction – General presentation. (2007). Materials and Structures, 40, 841-853.
[9] D.J. Naus, A Compilation of Elevated Temperature Concrete Material Property Data and Information for use in Assessments of Nuclear Power Plant Reinforced Concrete Structures (NUREG/CR-7031), US Nuclear Regulatory Commission, Washington, 2010.
[10] G.A. Khoury, Effect of fire on concrete and concrete structures, Prog. Struct. Mat. Eng. 4 (2) (2000) 429–447.
[11] O. Arioz, Effects of elevated temperatures on properties of concrete, Fire Saf. J. 42 (8) (2007) 516–522.
[12] L. Phan, N. Carino, Effects of test conditions and mixture proportions on behavior of high-strength concrete exposed to high temperatures, ACI Mater. J. 99 (1) (2002) 54–66.
[13] J.C. Marechal, Variations in the modulus of elasticity and Poisson's ratio with temperature, ACI Special Publ. 34 (1972) 495–504.
[14] I. Janotka, L. Bagel, Pore structures, permeabilities, and compressive strengths of concrete at temperatures up to 800 °C, ACI Mater. J. 99 (2) (2002) 196–200.
[15] J. Lee, Y. Xi, K. Willam, Properties of concrete after high-temperature heating and cooling, ACI Mater. J. 105 (4) (2008) 334–341.
[16] B. Zhang, Effects of moisture evaporation (weight loss) on fracture properties of high performance concrete subjected to high temperatures, Fire Saf. J. 46 (8) (2011) 543–549.
[17] A. Pineaud, P. Pimienta, S. Rémond, H. Carré, Mechanical properties of high performance self-compacting concretes at room and high temperature, Constr. Build. Mater. 112 (2016) 747–755.
[18] Y.F. Chang, Y.H. Chen, M.S. Sheu, G.C. Yao, Residual stress-strain relationship for concrete after exposure to high temperatures, Cement Concrete Res. 36 (10) (2006) 1999–2005.
[19] G. Baker, The effect of exposure to elevated temperatures on the fracture energy of plain concrete, Mater. Struct. 29 (19) (1996) 383–388.
[20] C.V. Nielsen, N. Bicanic, Residual fracture energy of high-performance and normal concrete subject to high temperatures, Mater. Struct. 36 (2003) 515–521.
[21] H. Fares, A. Noumowe, S. Remond, Self-consolidating concrete subjected to high temperature Mechanical and physicochemical properties, Cem. Concr. Res. 39 (2009) 1230–1238.
[22] G. Ye, X. Liu, G. De Schutter, L. Taerwe, P. Vandevelde, Phase distribution and microstructural changes of self-compacting cement paste at elevated temperature, Cem. Concr. Res. 37 (6) (2007) 978–987.
[23] J. Tao, X. Liu, Y. Yuan, L. Taerwe, Transient strain of self-compacting concrete loaded in compression heated to 700 C, Mater. Struct. 46 (1–2) (2013) 191–201.
[24] K. Pistol, F. Weise, B. Meng, High temperature behaviour of self-compacting concrete with limestone powder. In Rheology and Processing of Construction Materials: Proceedings of the 7th RILEM International Conference on Self-Compacting Concrete and 1st RILEM International Conference on Rheology and Processing of Construction Materials, RILEM Proceedings PRO 90 (pp. 221-228). RILEM Bagneux (2013).
[25] Dimitrios G. Aggelis, Tomoki Shiotani, Shouhei Momoki, Akinobu Hirama, Acoustic emission and ultrasound for damage characterization of concrete elements, ACI Mater. J. 106 (6) (2009) 1–6.
[26] ASTM E1316–17a: Standard Terminology for Nondestructive Examinations, ASTM International, Books of Standards, West Conshohocken, PA, 2017.
[27] C.U. Grosse, M. Ohtsu, Acoustic Emission Testing, Springer-Verlag, Berlin Heidelberg, 2008.
[28] R.V. Sagar, B.K.R. Prasad, An experimental study on acoustic emission energy as a quantitative measure of size independent specific fracture energy of concrete beams, Constr. Build. Mater. 25 (5) (2011) 2349–2357.
[29] Q. Dai, K. Ng, J. Zhou, E.L. Kreiger, T.M. Ahlborn, Damage investigation of single-edge notched beam tests with normal strength concrete and ultra high performance concrete specimens using acoustic emission techniques, Constr. Build. Mater. 31 (2012) 231–242.
[30] K. Ohno, K. Uji, A. Ueno, M. Ohtsu, Fracture process zone in notched concrete beam under three-point bending by acoustic emission, Constr. Build. Mater. 67 (2014) 139–145.

[31] J. Saliba, A. Loukili, J.P. Regoin, D. Grégorie, L. Verdon, G. Pijaudier-Cabot, Experimental analysis of crack evolution in concrete by the acoustic emission technique, Frattura e Integritá Strutturale 34 (2015) 300–308.
[32] S. De Sutter, S. Verbruggen, T. Tysmans, D.G. Aggelis, Fracture monitoring of lightweight composite-concrete beams, Compos. Struct. 167 (2017) 11–19.
[33] M. Ohtsu, M. Uchida, T. Okamoto, S. Yuyama, Damage assessment of reinforced concrete beams qualified by acoustic emission, ACI Struct. J. 99 (4) (2002) 411–417.
[34] RILEM Technical Committee 212-ACD: Test method for damage qualification of reinforced concrete beams by acoustic emission. (2010). Materials and Structures, 43, 1183-1186.
[35] P. Ziehl, A. Ridge, Evaluation of strengthened RC beams: cyclic load test and acoustic emission methods, ACI Struct. J. 103 (6) (2006) 832–841.
[36] Z. Liu, P. Ziehl, Evaluation of reinforced concrete beam specimens with acoustic emission and cyclic load test methods, ACI Struct. J. 106 (3) (2009) 288–299.
[37] S. Colombo, M.C. Forde, I.G. Main, M. Shigeishi, Predicting the ultimate bending capacity of concrete beams from the "relaxation ratio" analysis of AE signals, Constr. Build. Mater. 19 (2005) 746–754.
[38] T. Schumacher, C.C. Higgins, S.C. Lovejoy, Estimating operating load conditions on reinforced concrete highway bridges with b-value analysis from acoustic emission monitoring, Struct. Health Monitor. 10 (1) (2011) 17–32.
[39] R.V. Sagar, M.V.M.S. Rao, An experimental study on loading rate effect on acoustic emission based b-values related to reinforced concrete fracture, Constr. Build. Mater. 70 (2014) 460–472.
[40] M.E. Zitto, R. Piotrkowski, A. Gallego, F. Sagasta, A. Benavent-Climent, Damage assessed by wavelet scale bands and b-value in dynamical tests of a reinforced concrete slab monitored with acoustic emission, Mech. Syst. Sig. Process. 60 (2015) 75–89.
[41] T. Shiotani, J. Bisschop, J.G.M. Van Mier, Temporal and spatial development of drying shrinkage cracking in cement-based materials, Eng. Fract. Mech. 70 (2003) 1509–1525.
[42] A. Behnia, H.K. Chai, T. Shiotani, Advanced structural health monitoring of concrete structures with the aid of acoustic emission, Constr. Build. Mater. 65 (2014) 282–302.
[43] M. Ohtsu, Acoustic Emission (AE) and Related Non-destructive Evaluation (NDE) Techniques in the Fracture Mechanics of Concrete – Fundamentals and Applications, Woodhead Publishing, Cambridge, 2015.
[44] K. Ohno, M. Ohtsu, Crack classification in concrete based on acoustic emission, Constr. Build. Mater. 24 (2010) 2339–2346.
[45] D.G. Aggelis, Classification of cracking mode in concrete by acoustic emission parameters, Mech. Res. Commun. 38 (2011) 153–157.
[46] A. Farhidzadeh, A.C. Mpalaskas, T.E. Matikas, H. Farhidzadeh, D.G. Aggelis, Fracture mode identification in cementitious materials using supervised pattern recognition of acoustic emission features, Constr. Build. Mater. 67 (2014) 129–138.
[47] A. Behnia, H.K. Chai, M. Yorikawa, S. Momoki, M. Terazawa, T. Shiotani, Integrated non-destructive assessment of concrete structures under flexure by acoustic emission and travel time tomography, Constr. Build. Mater. 67 (2014) 202–215.
[48] B. Chen, J. Liu, Experimental study on AE characteristics of three-point-bending concrete beams, Cem. Concr. Res. 34 (3) (2004) 391–397.
[49] D. Soulioti, N.M. Barkoula, A. Paipetis, T.E. Matikas, T. Shiotani, D.G. Aggelis, Acoustic emission behavior of steel fibre reinforced concrete under bending, Constr. Build. Mater. 23 (12) (2009) 3532–3536.
[50] D.G. Aggelis, D.V. Soulioti, N. Sapouridis, N. Barkoula, A. Paipetis, T. Matikas, Acoustic emission characterization of the fracture process in fibre reinforced concrete, Constr. Build. Mater. 25 (11) (2011) 4126–4131.
[51] D.G. Aggelis, D.V. Soulioti, E.A. Gatselou, N.-M. Barkoula, T.E. Matikas, Monitoring of the mechanical behavior of concrete with chemically treated steel fibers by acoustic emission, Constr. Build. Mater. 48 (2013) 1255–1260.
[52] C. Grosse, J. Ožbolt, R. Richter, G. Periškić, Acoustic emission analysis and thermo-hygro-mechanical model for concrete exposed to fire, J. Acoustic Emission 28 (2010) 188–203.
[53] M. Ozawa, S. Uchida, T. Kamada, H. Morimoto, Study of mechanisms of explosive spalling in high-strength concrete at high temperatures using acoustic emission, Constr. Build. Mater. 37 (2012) 621–628.
[54] M.L. Heap, A. Laumann, K.-U. Hess, P. Meredith, D. Dingwell, S. Huismann, The influence of thermal-stressing (up to 1000 °C) on the physical, mechanical, and chemical properties of siliceous-aggregate, high-strength concrete, Constr. Build. Mater. 42 (2013) 248–465.
[55] J. Geng, Q. Sun, W. Zhang, C. Lü, Effect of high temperature on mechanical and acoustic emission properties of calcareous-aggregate concrete, Appl. Therm. Eng. 106 (2016) 1200–1208.
[56] H. Xargay, P. Folino, L. Sambataro, G. Etse, Temperature effects on failure behavior of self-compacting high strength plain and fiber reinforced concrete, Constr. Build. Mater. 165 (2018) 723–734.
[57] A. Caggiano, H. Xargay, P. Folino, E. Martinelli, Experimental and numerical characterization of the bond behavior of steel fibers recovered from waste tires embedded in cementitious matrices, Cem. Concr. Compos. 62 (2015) 146–155.
[58] RILEM Technical Committee 162-TDF: Test and design methods for steel fibre reinforced concrete – Bending test. (2002). Materials and Structures, 35, 579–582.
[59] A. Caggiano, S. Gambarelli, E. Martinelli, N. Nisticò, M. Pepe, Experimental characterization of the post-cracking response in Hybrid Steel/Polypropylene Fiber-Reinforced Concrete, Constr. Build. Mater. 125 (2016) 1035–1043.
[60] RILEM Technical Committee 50-FMC: Determination of fracture energy of mortar and concrete by means of three point bend tests on notched beams, Mater. Struct. 18 (106) (1985) 285–290.
[61] A. Pollock, Acoustic emission inspection, Technical report, TR-103-96-12/89, Physical Acoustics corporation, 195 Clarksville Road, Princeton Jct., NJ., USA (1989).
[62] P. Rossi, J.L. Robert, J.P. Gervais, D. Bruhat, Acoustic emission applied to study crack propagation in concrete, Mater. Struct. 22 (1989) 374–384.
[63] ACI Committee 224 – ACI 224R-01. (2001). Control of cracking in concrete structures. Reported by ACI Committee 244.
[64] RILEM Technical Committee 212-ACD: Test method for classification of active cracks in concrete structures by acoustic emission. (2010). Materials and Structures, 43, 1187-1189.
[65] WIRAND®,, FS3N, Steel fibres for concrete, Maccaferri Technical, Data Sheet (2010).
[66] FIBROMAC12®, Mono-filamentary polypropylene fibre, Maccaferri Technical Data Sheet, 2010.